

Polymethylmethacrylate (PMMA) Material Test Results for the Capillary Flow Experiments (CFE)

Bradley A. Lerch
Glenn Research Center, Cleveland, Ohio

John C. Thesken
Ohio Aerospace Institute, Brook Park, Ohio

Charles T. Bunnell
ZIN Technologies, Inc., Brook Park, Ohio

NASA STI Program . . . in Profile

Since its founding, NASA has been dedicated to the advancement of aeronautics and space science. The NASA Scientific and Technical Information (STI) program plays a key part in helping NASA maintain this important role.

The NASA STI Program operates under the auspices of the Agency Chief Information Officer. It collects, organizes, provides for archiving, and disseminates NASA's STI. The NASA STI program provides access to the NASA Aeronautics and Space Database and its public interface, the NASA Technical Reports Server, thus providing one of the largest collections of aeronautical and space science STI in the world. Results are published in both non-NASA channels and by NASA in the NASA STI Report Series, which includes the following report types:

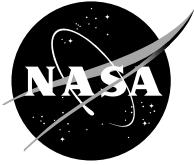
- **TECHNICAL PUBLICATION.** Reports of completed research or a major significant phase of research that present the results of NASA programs and include extensive data or theoretical analysis. Includes compilations of significant scientific and technical data and information deemed to be of continuing reference value. NASA counterpart of peer-reviewed formal professional papers but has less stringent limitations on manuscript length and extent of graphic presentations.
- **TECHNICAL MEMORANDUM.** Scientific and technical findings that are preliminary or of specialized interest, e.g., quick release reports, working papers, and bibliographies that contain minimal annotation. Does not contain extensive analysis.
- **CONTRACTOR REPORT.** Scientific and technical findings by NASA-sponsored contractors and grantees.

- **CONFERENCE PUBLICATION.** Collected papers from scientific and technical conferences, symposia, seminars, or other meetings sponsored or cosponsored by NASA.
- **SPECIAL PUBLICATION.** Scientific, technical, or historical information from NASA programs, projects, and missions, often concerned with subjects having substantial public interest.
- **TECHNICAL TRANSLATION.** English-language translations of foreign scientific and technical material pertinent to NASA's mission.

Specialized services also include creating custom thesauri, building customized databases, organizing and publishing research results.

For more information about the NASA STI program, see the following:

- Access the NASA STI program home page at <http://www.sti.nasa.gov>
- E-mail your question via the Internet to help@sti.nasa.gov
- Fax your question to the NASA STI Help Desk at 301-621-0134
- Telephone the NASA STI Help Desk at 301-621-0390
- Write to:
NASA Center for AeroSpace Information (CASI)
7115 Standard Drive
Hanover, MD 21076-1320



Polymethylmethacrylate (PMMA) Material Test Results for the Capillary Flow Experiments (CFE)

Bradley A. Lerch
Glenn Research Center, Cleveland, Ohio

John C. Thesken
Ohio Aerospace Institute, Brook Park, Ohio

Charles T. Bunnell
ZIN Technologies, Inc., Brook Park, Ohio

National Aeronautics and
Space Administration

Glenn Research Center
Cleveland, Ohio 44135

Acknowledgments

The authors would like to thank Dr. Liu for personal communications regarding his Brazilian disk test methods, Mr. C. Burke for performing the experiments, and Dr. L. Ghosn for his valuable technical comments. We also appreciate the interaction with the CFE Team: J. Mark Hickman/GRC (Project Manager), Bob Green/GRC (Project Scientist), Mark Weislogel/Portland State University (Principal Investigator), Dan Gotti/NCMR (Design Engineer), and ZIN Technologies, Inc., team members: Carol Kurta (Task Lead), Mike Sydenstricker (Integration), Deb Lyden (Quality Assurance), and Ray Margie (Technician). This work was funded by PT Exploration Systems Division of the Life Support and Habitation/Exploration Systems.

Trade names and trademarks are used in this report for identification only. Their usage does not constitute an official endorsement, either expressed or implied, by the National Aeronautics and Space Administration.

Level of Review: This material has been technically reviewed by technical management.

Available from

NASA Center for Aerospace Information
7115 Standard Drive
Hanover, MD 21076-1320

National Technical Information Service
5285 Port Royal Road
Springfield, VA 22161

Available electronically at <http://gltrs.grc.nasa.gov>

Polymethylmethacrylate (PMMA) Material Test Results for the Capillary Flow Experiments (CFE)

Bradley A. Lerch
National Aeronautics and Space Administration
Glenn Research Center
Cleveland, Ohio 44135

John C. Thesken
Ohio Aerospace Institute
Brook Park, Ohio 44142

Charles T. Bunnell
ZIN Technologies, Inc.
Brook Park, Ohio 44142

Summary

In support of the Capillary Flow Experiments (CFE) program, several polymethylmethacrylate (PMMA) flight vessels were constructed. Some vessels used a multipiece design, which was chemically welded together. Due to questions regarding the effects of the experiment fluid (silicone oil) on the weld integrity, a series of tests were conducted to provide evidence of the adequacy of the current vessel design. Tensile tests were conducted on PMMA samples that were both in the as-received condition, and also aged in air or oil for up to 8 weeks. Both welded and unwelded samples were examined. Fracture of the joints was studied using notched tensile specimens and Brazilian disk tests. Results showed that aging had no effect on tensile properties. While the welded samples were weaker than the base parent material, the weld strength was found to be further degraded by bubbles in the weld zone. Finally, a fracture analysis using the worst-case fracture conditions of the vessel was performed, and the vessel design was found to have a factor of three safety margin.

Introduction

The NASA Glenn Research Center (GRC) Capillary Flow Experiments (CFE) program is developing microgravity experiment payloads to explore fluid interfaces in microgravity on the International Space Station (ref. 1). The information to be gained from CFE is relevant to the design of fluid-bearing systems in which capillary forces predominate, for example, in the passive positioning of liquids in spacecraft fuel tanks.

To achieve the science goals of CFE, several types of experiment vessels are constructed. One type of vessel is known as the interior corner flow (ICF). The multipiece ICF vessel (fig. 1), which comprises the test chamber, and the fluid reservoir is made of polymethylmethacrylate (PMMA) per ASTM D-4802 (ref. 2). One of the key reasons PMMA was selected was its excellent optical properties. The CFE science data collection consists of digital video imagery of the capillary fluid flow inside the test chamber, and good visual access is required.

The fabricator of the vessel used methylene chloride to solvent bond (“chemically weld”) the multiple pieces together. This chemical is a solvent that dissolves the plastic surface, allowing the pieces to flow together. The solvent evaporates leaving a tight seal and bond. Of the CFE hardware, only the ICF vessel is a multiple piece PMMA construction that uses methylene chloride for bonding the PMMA. The other CFE vessels, Contact Line and Vane Gap, use single piece PMMA construction that does not have any of these bonds. The bonding method of manufacture for ICF was necessary to meet the particular test chamber geometry requirements.

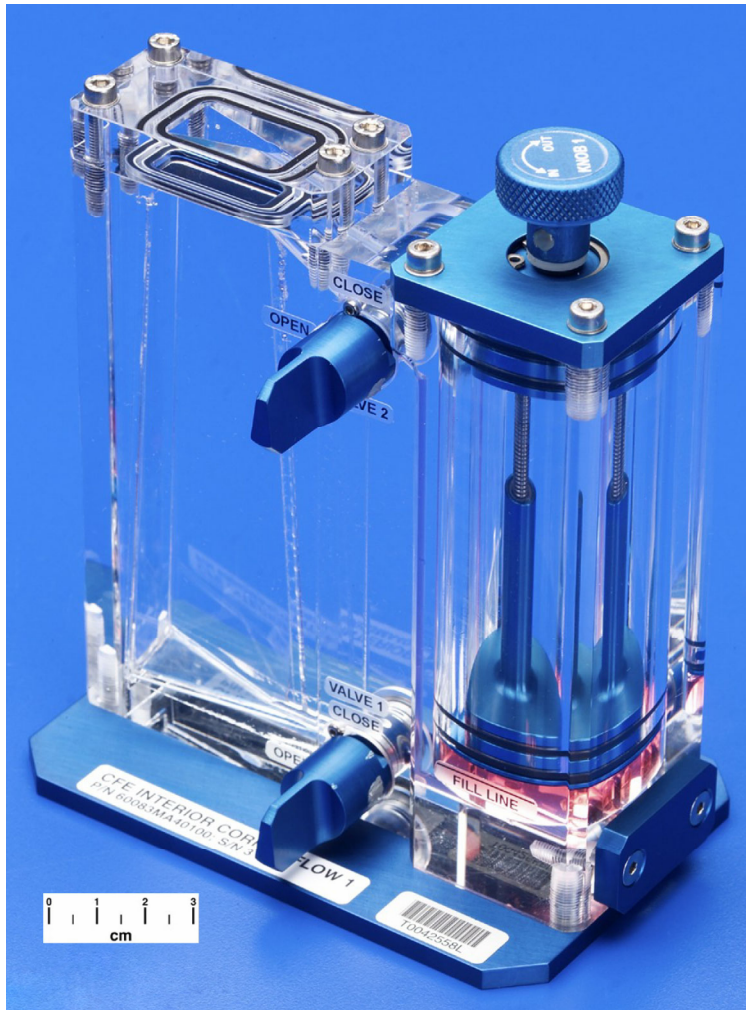


Figure 1.—CFE interior corner flow vessel.

The experimental fluid used in CFE is silicone oil of differing viscosities. The ICF vessels will use silicone oil viscosities of 2 cSt and 5 cSt. CFE conversations with the NASA Johnson Space Center (JSC) Payload Safety Review Panel (PSRP) indicated some past experience with adhesive bonded plastic where experiment fluid significantly degraded the adhesive to the point of failure. It was not clear what the plastic was, though it could have been PMMA. Hence, a question arose about the effect of silicone oil on the CFE solvent bonded PMMA joint.

In response to the JSC PSRP concerns, CFE, in conjunction with the GRC Structures Division, developed and initiated a PMMA materials test plan. This test plan is documented in CFE-TPRO-017—CFE PMMA Test Procedure (ZIN Technologies, Inc., report). The primary issues addressed by the tests are (1) the strength of the bonded PMMA material in relation to the parent material and (2) the effect of silicone oil on the strength of the bonded material.

To assess the joint strength a number of different tests were conducted. These included tests on the PMMA itself, tests on welded PMMA, and notched samples of both welded and unwelded PMMA. Additionally, samples were aged in either air or silicone oil for up to 8 weeks to investigate any potential effects of PMMA aging or interaction with the silicone oil. This report documents the results of tests conducted by the GRC Structures Division as part of the requirements of CFE-TPRO-017.

Experiments

Material

All specimens used in this study and the flight vessels were taken from one block of PMMA, which was procured by ZIN Technologies, Inc. The block was 152 mm (6 in.) thick, 508 mm (20 in.) wide, and 3050 mm (120 in.) in length. It was sectioned and then machined down to the desired sample thicknesses and polished to obtain visually transparent, scratch-free surfaces.

Tensile Tests

Tensile tests were conducted on PMMA samples according to ASTM D638 (ref. 3). The samples were 165-mm- (6.5-in.-) long dogbone-shaped samples with a 3.5 mm (0.138 in.) thickness (Type I samples in ASTM D638). A few samples having a 10.0 mm (0.394 in.) thickness were also tested, but only in the unsoaked, welded state. This thickness represented the thickness of the plates in the actual component. The thicker samples were used as a conservative case (anticipated lower tensile properties) representing more of a plane strain situation. Tests were conducted in air and at 20 °C on a 20 kip, hydraulically actuated load frame in Glenn's Fatigue and Structures Technology (FAST) Lab. The tests were run in strain control and loaded at a constant strain rate of 0.0025/s. A 12.7 mm (0.5 in.) gage length extensometer was used to measure strains, and a load cell measured the applied loads. Both test control and data acquisition were performed using a dedicated PC. The digital data were analyzed with a commercially available program, CESLab, which is used for most test data analysis in the Life Prediction Branch at Glenn. All equipment was calibrated according to standard FAST Lab quality procedures.

Samples 3.5 mm (0.138 in.) thick were tested in the as-received condition, as well as after aging for 2, 4, and 8 weeks. Samples were aged either in air or in silicone oil. The oil-soaked samples were cleaned with a dry cloth before testing. All samples were visually inspected before testing to document any damage which might affect the test results. This was especially necessary for the welded samples, as will be described later.

Testing was also performed on double-edged notched samples (design nos. 80006 and 80008), which had a similar dogbone design as the unnotched samples, but had a thickness of 6.0 mm (0.236 in.). These samples were used to give an idea of the notch sensitivity of both the PMMA material and the welded joint. In particular we were simulating the effects of the glue reservoir. The reservoir catches excess glue in the joint to ensure complete bonding. The reservoir is a 1.5 mm (0.06 in.) diameter groove placed 1.5 mm (0.06 in.) from the interior edge of the bonded surface. Conservatively assuming that the inner 1.5 mm is not bonded, this gives a notch that is 1.5 mm (0.06 in.) wide and 3.0 mm (0.118 in.) long, which was the notch size used in test samples. For the welded specimens (80006) the weld was placed (due to manufacturing convenience) at the upper edge of the notch (fig. 2). The notched samples were tested only in the unsoaked condition.

Generally, triplicate tests were conducted per condition. However, more tests were occasionally run to answer questions as they arose. Table I gives the final test matrix for all the tensile specimens. The soaked specimens include both air (threesamples) and oil (three samples) as soaking media. Soaking of samples in air acted as a control condition for the oil-soaked samples and also ensured that properties of the PMMA did not change with time.

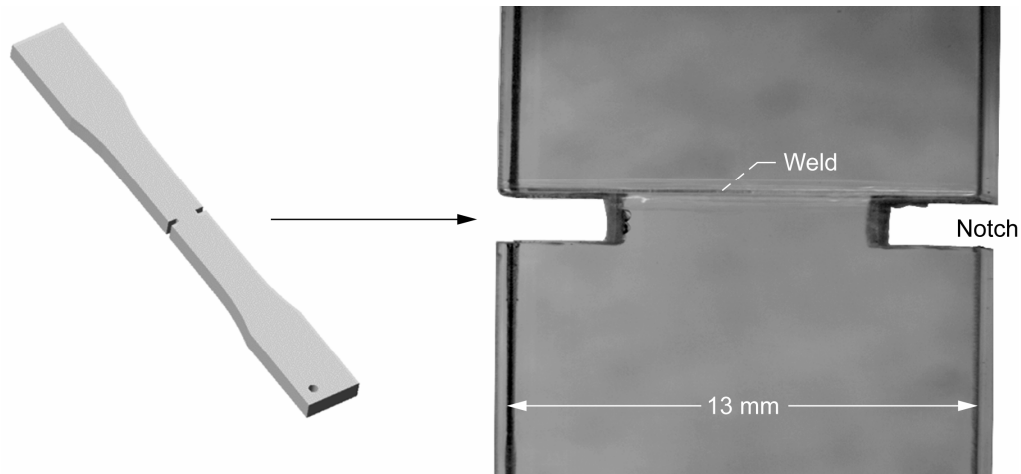


Figure 2.—Double-edged notch sample with weld.

TABLE I.—FINAL TENSILE TEST MATRIX

Sample type	Tensile curves							
	Unsoaked billet		Soaked billet		Unsoaked weld		Soaked weld	
	No. of samples	Drawing no.	No. of samples	Drawing no.	No. of samples	Drawing no.	No. of samples	Drawing no.
No age	3	80003	None		4	80004	None	
2 weeks	3	80003	3	80003	3	80004	3	80004
4 weeks	3	80003	3	80003	3	80004	3	80004
8 weeks	3	80003	3	80003	3	80004	3	80004
Thick weld—no age	None		None		6	80007	None	
Notched sample—no age	3	80008	None		3	80006	None	
Brazilian disk—no age	6	80010	None		6	80011	None	

Brazilian Disk Tests

The Brazilian disk test was used to gain insight into the modes I and II fracture properties of the material. The disk contains a center crack symmetrically located and is loaded in compression between two platens. The included angle between the crack plane and the line of applied load determines the fracture mode of the specimen. The approach follows work done by Liu and coworkers (ref. 4) at Lawrence Livermore Laboratory on enhanced shear banding in epoxy specimens. Liu et al. utilized the closed-form solution developed by Atkinson et al. (ref. 5) to generate the required specimen calibration factors. The specimens used here are dimensioned identically so the analytical results published by Liu et al. (ref. 4) may be used to calibrate these specimens and determine appropriate angles for pure modes I and II. The PMMA disks were machined to 6 mm (0.236 in.) thick and had a diameter of 38 mm (1.5 in.). A center notch 19 mm (0.748 in.) in length and 0.6 mm (0.025 in.) in width was machined into the center of the sample (figure in table III). A starter crack was introduced at each end of the notch using a scalpel. The starter crack was approximately 0.2 mm (0.008 in.) in length. For the welded samples, the notch was supposed to be centered with respect to the weld joint. However, machining often led to the weld joint being parallel to the upper surface of the notch.

The disks were placed between two steel plates fixed to the grips of a hydraulically actuated load frame, similar to the one used for the tensile samples. The notch was placed vertically (parallel to the load axis) for mode I tests and placed at a 22.5° angle to vertical for the mode II tests, and compression loads were applied. The tests were run in stroke control and at a crosshead displacement rate of 0.05 mm/s (0.002 in./s). Tests were conducted in air and at 20 °C. Only as-received material was tested. Soaking was not performed on these samples.

Results

Tensile Specimens

Visual examination of the samples revealed them to be optically transparent and free of major scratches and defects. The exception to this observation was that many of the welded samples contained defects (“bubbles”) in the weld. The size and distribution of these bubbles varied from specimen to specimen as shown in figure 3. These bubbles are not uncommon with these welds and have been observed previously. In fact, examination of the flight hardware shows significant bubbles in the weld zones. Specimens with weld defects were not used for determination of the property averages from triplicate tests. However, additional specimens containing bubbles were tested to give a qualitative ranking of the effect of bubbles on tensile properties.

Typical tensile curves are shown in figure 4 for the unsoaked, no-aged samples (billet and welded). In general, the billet samples (as-received) exhibited good ductility and strength. The curve was linear at low strain and progressed into a smooth yield. The welded samples had less strength and ductility. Typical tensile parameters are indicated in the figure and are tabularized for each sample in table II. Note that the failure stress in the table is given by the net section stress for the notched samples. Specimens highlighted in yellow have bubble-containing weld joints. Photographs of the weld joint of these samples showing the bubbles are also shown in the table.

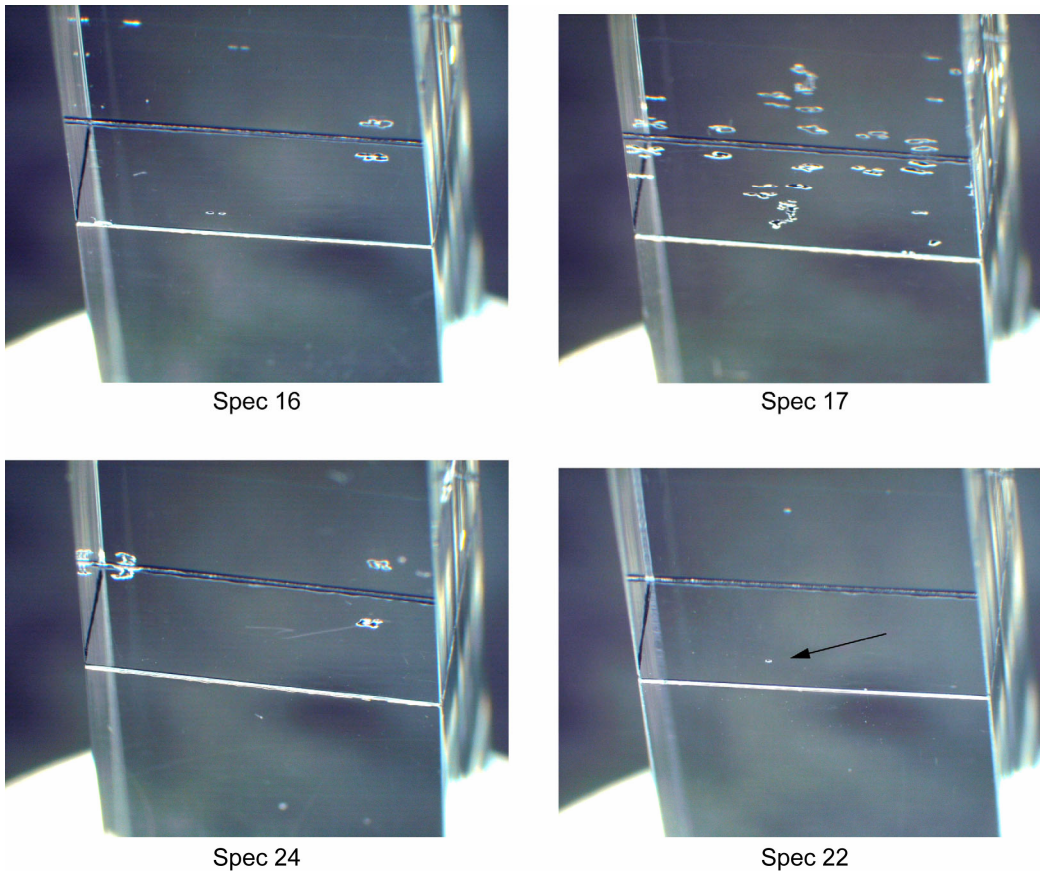


Figure 3.—Bubbles in weld joint.

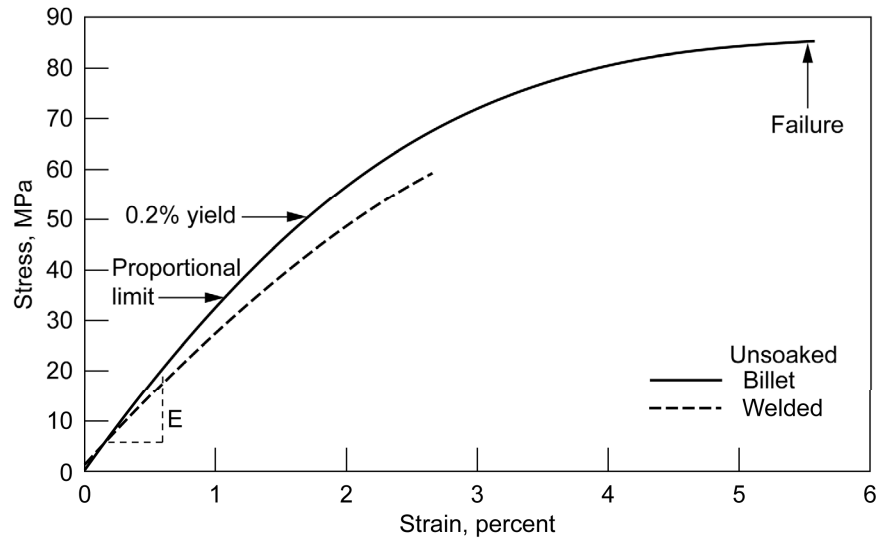


Figure 4.—Typical tensile curves for welded and unwelded samples.

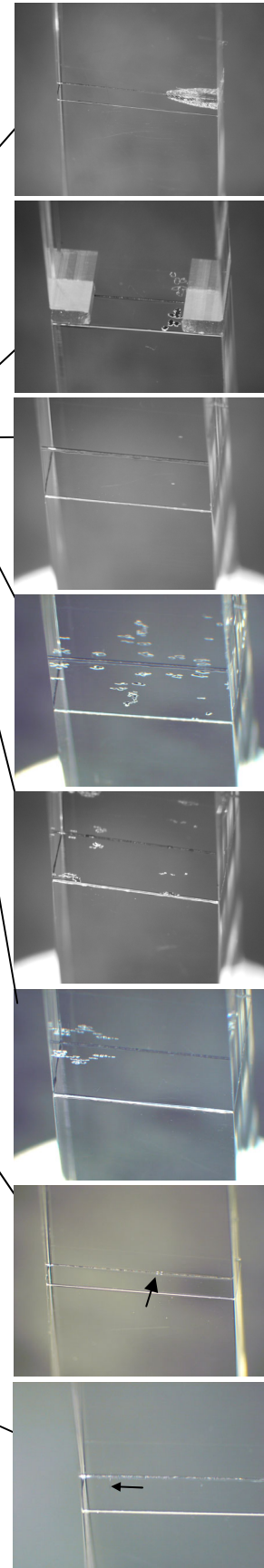
Bar graphs of three tensile parameters are shown in figures 5 through 7. These parameters are given for the triplicate tests and for each condition. Data for selected specimens containing weld bubbles are included in the bar graphs. Those particular specimens were chosen to show the largest range of properties for bubble-containing samples. Values for the remaining bubble-containing samples were not plotted for clarity reasons, but are given in table II. In each of the plots, the identical legend scheme is used. The data are divided into three groups, representing the three repeats. The leftmost bars in each group are colored blue and represent the unwelded billet material. Immediately to the right of these bars is a red-colored group, which represents welded material. The remaining two bars in the group are cream colored and depict the data for the notched samples, both unwelded and welded. The various soaking conditions are depicted by different background patterns and are described in the legend. Since the thick (10 mm (0.394 in.)) samples were only tested in the welded state, they only appear in the red group of data. Note that there are arrows above some of the bars. This denotes that the data were from defect-containing samples.

Values for elastic modulus are given in figure 5. There appears to be no obvious effect of the weld joint, or soaking on the elastic modulus. There is also no effect of defects (bubbles or notches) on the modulus. Pooling all data listed in table II, the average modulus is 3.1 ± 0.3 GPa, (446 ± 42 ksi) where the variation represents one standard deviation. This average value is typical for the modulus of PMMA (ref. 6).

Values for the maximum or failure stress are given in figure 6. By visual inspection, there is no effect of soaking either in air or oil on the failure stress. This is true for both unwelded and welded samples. Given this, pooling of all data for the unwelded samples yields an average strength of 85 ± 1 MPa (12.3 ± 0.2 ksi), and this is slightly higher than values reported (ref. 6) for PMMA material. It is obvious that by introducing the weld into the samples, the strength drops by 32 percent to an average of 58 ± 2 MPa (8.4 ± 0.3 ksi). It should be noted that all of the welded samples fractured in the weld and not in the parent material, indicating that the strength of the joint is weaker than the parent material. The notched samples are still weaker, having an average strength of 41 ± 2 MPa (5.9 ± 0.3 ksi). There was no apparent difference in strength between the welded and unwelded notched samples. The welded, notched samples broke in the notch. However, each sample had a different amount of crack surface contained in the weld, from 0 to 100 percent. There was no effect of soaking the samples in either air or oil on the welded, unnotched samples. However, there can be a strength decrease due to the introduction of bubbles into the welds. This is evident in both the unnotched and notched samples. In the worst case observed, the strength of a welded sample (specimen no. 82) dropped to 13 MPa (1.9 ksi), which is a 76 percent drop in strength compared to the average for the defect-free, welded samples.

TABLE II.—SUMMARY OF TENSILE TESTS

Spec. no.	Geometry	Spec design	Pre-condition	E, MPa	Property limit, MPa	YS 0.2%, MPa	Failure stress, MPa	Failure strain, %
As-received								
37	Smooth, unwelded	80003	Unsoaked	3.2	33.4	52.5	85.3	5.6
38	Smooth, unwelded	80003	Unsoaked	3.3	25.3	49.9	82.1	4.0
39	Smooth, unwelded	80003	Unsoaked	3.1	32.5	52.1	87.3	5.0
82	Smooth, welded	80004	Unsoaked	3.4	4.8	11.8	12.8	0.5
83	Smooth, welded	80004	Unsoaked	2.7	21.7	44.8	59.3	2.8
84	Smooth, welded	80004	Unsoaked	2.8	23.4	45.2	59.2	2.7
109	Smooth, welded	80004	Unsoaked	2.7	22.5	44.7	58.3	2.7
25	Notched, unwelded	80008	Unsoaked	3.4	23.6	-----	42.7	1.4
26	Notched, unwelded	80008	Unsoaked	3.4	17.9	40.0	40.1	1.3
27	Notched, unwelded	80008	Unsoaked	3.4	18.7	-----	41.3	1.3
1	Notched, welded	80006	Unsoaked	3.2	19.9	-----	40.7	1.4
2	Notched, welded	80006	Unsoaked	3.6	17.7	-----	37.9	1.2
3	Notched, welded	80006	Unsoaked	3.5	11.4	-----	24.1	0.8
13	Thick, welded	80007	Unsoaked	3.1	19.6	-----	45.3	1.7
17	Thick, welded	80007	Unsoaked	3.8	17.8	-----	27.8	0.8
18	Thick, welded	80007	Unsoaked	3.4	24.1	49.4	58.2	2.1
23	Thick, welded	80007	Unsoaked	3.2	24.1	48.8	51.0	1.8
14	Thick, welded	80007	Unsoaked	3.7	16.7	-----	31.8	0.9
21	Thick, welded	80007	Unsoaked	3.6	15.4	-----	31.9	1.0
2 weeks age								
40	Smooth, unwelded	80003	Unsoaked	2.9	31.9	51.0	84.5	5.9
41	Smooth, unwelded	80003	Unsoaked	3.1	33.1	51.9	85.5	6.6
42	Smooth, unwelded	80003	Unsoaked	2.8	30.7	50.1	85.2	6.4
43	Smooth, unwelded	80003	Oil soaked	2.9	32.3	51.5	86.3	6.8
44	Smooth, unwelded	80003	Oil soaked	3.0	32.8	51.5	86.8	6.9
45	Smooth, unwelded	80003	Oil soaked	2.9	38.3	51.3	85.8	6.1
85	Smooth, welded	80004	Unsoaked	2.9	22.5	46.1	57.9	2.4
86	Smooth, welded	80004	Unsoaked	2.8	22.1	46.1	59.1	2.6
87	Smooth, welded	80004	Unsoaked	2.7	22.3	44.4	58.1	2.6
90	Smooth, welded	80004	Oil soaked	2.9	25.0	46.5	59.5	2.5
88	Smooth, welded	80004	Oil soaked	3.0	23.7	46.4	60.3	2.5
89	Smooth, welded	80004	Oil soaked	2.9	26.2	47.4	60.3	2.5
4 weeks age								
48	Smooth, unwelded	80003	Unsoaked	2.8	31.8	49.8	83.2	7.9
49	Smooth, unwelded	80003	Unsoaked	3.1	33.2	52.4	84.7	6.7
50	Smooth, unwelded	80003	Unsoaked	2.8	32.0	50.2	82.4	8.5
51	Smooth, unwelded	80003	Oil soaked	3.1	31.9	52.7	85.4	7.1
52	Smooth, unwelded	80003	Oil soaked	2.9	33.0	50.7	84.4	8.2
53	Smooth, unwelded	80003	Oil soaked	2.9	32.5	51.1	84.9	6.9
93	Smooth, welded	80004	Unsoaked	2.8	23.4	46.3	59.5	2.6
94	Smooth, welded	80004	Unsoaked	3.0	23.0	47.2	58.0	2.3
95	Smooth, welded	80004	Unsoaked	2.8	24.1	45.3	57.9	2.6
96	Smooth, welded	80004	Oil soaked	3.1	22.8	48.1	53.6	2.0
97	Smooth, welded	80004	Oil soaked	2.8	24.1	47.4	58.4	2.5
98	Smooth, welded	80004	Oil soaked	2.7	26.2	44.3	57.6	2.6
8 weeks age								
56	Smooth, unwelded	80003	Unsoaked	2.9	30.0	49.9	81.0	5.2
57	Smooth, unwelded	80003	Unsoaked	3.1	31.0	51.5	83.4	5.6
58	Smooth, unwelded	80003	Unsoaked	3.1	32.1	50.9	81.8	5.3
59	Smooth, unwelded	80003	Oil soaked	3.3	33.2	53.7	85.2	5.2
60	Smooth, unwelded	80003	Oil soaked	3.2	33.6	52.6	86.0	7.5
61	Smooth, unwelded	80003	Oil soaked	3.2	31.1	53.9	85.5	6.3
101	Smooth, welded	80004	Unsoaked	3.1	24.1	47.5	58.0	2.3
102	Smooth, welded	80004	Unsoaked	3.1	23.3	46.7	57.4	2.2
103	Smooth, welded	80004	Unsoaked	3.1	22.0	44.7	57.3	2.3
104	Smooth, welded	80004	Oil soaked	3.2	28.4	49.9	57.7	2.1
105	Smooth, welded	80004	Oil soaked	3.3	22.6	49.0	58.0	2.1
106	Smooth, welded	80004	Oil soaked	3.2	23.4	48.1	59.4	2.3



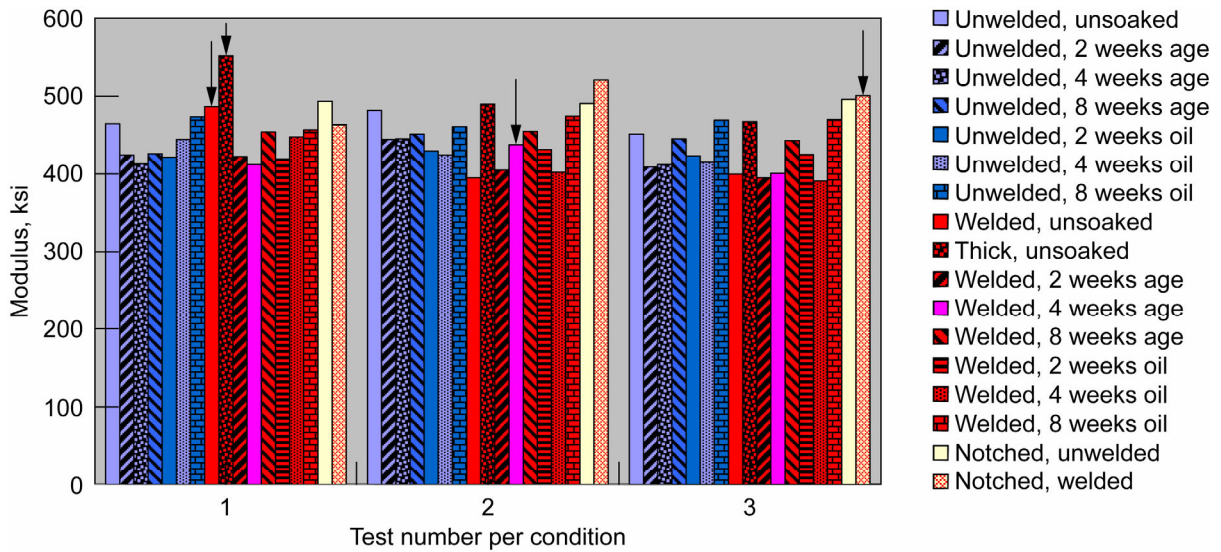


Figure 5.—Elastic modulus as a function of test condition. Modulus (arrows indicate specimens with bubbles in welds).

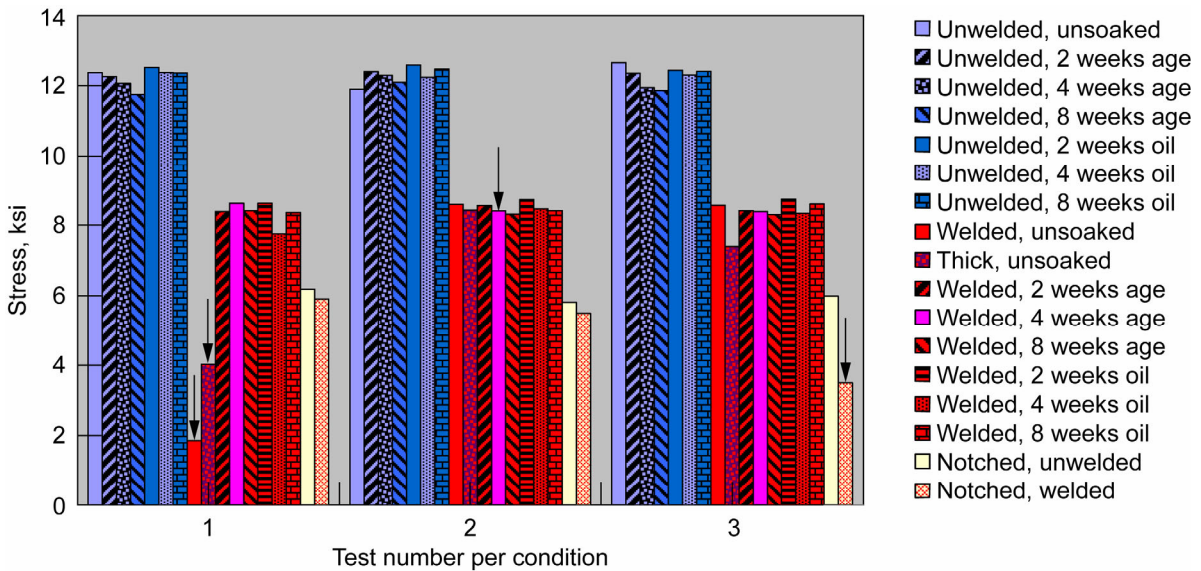


Figure 6.—Maximum strength for various test conditions. Net section failure stress (arrows indicate specimens with bubbles in welds).

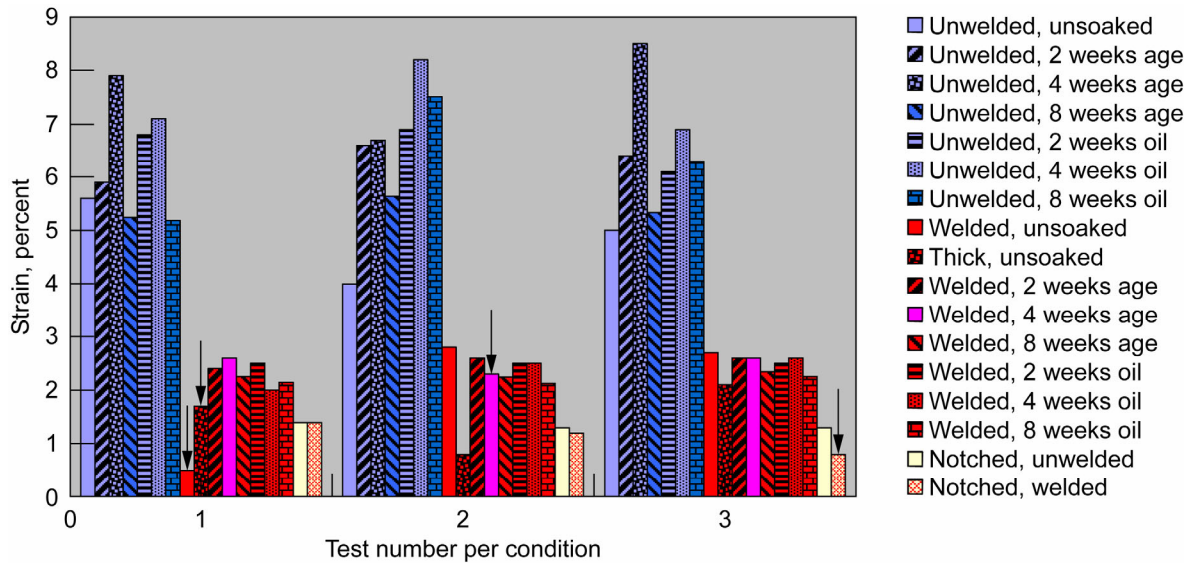


Figure 7.—Failure strain for various test conditions. Failure strain (arrows indicate specimens with bubbles in welds).

Figure 7 shows the failure strain for various test conditions. There was no observable effect of soaking in either air or oil on the failure strain. For the unwelded samples, the failure strains range from 4.0 to 8.5 percent with an average of 6.6 ± 1.2 percent. Introduction of a weld reduces the failure strain by 64 percent to an average of 2.4 ± 0.3 percent. An addition of defects, either weld bubbles or notches can reduce the failure strain even more. The lowest failure strain observed in this investigation was 0.5 percent for sample number 82. This sample failed immediately after yielding, that is, the stress-strain curve was approximately linear.

Brazilian Disk Specimens

The objective of these experiments was to appraise the fracture toughness of the unwelded and welded PMMA as a function of loading mode. Since the ICF vessel contains notches, in particular the glue-reservoirs at the weld lines, we were concerned about the stress amplification out of those notches. A conservative approach would be to approximate these notches as sharp cracks. If it can then be shown that the sharp cracks have sufficient toughness, then the notches in the vessel should be benign. While mode I cracking is the easiest to test and analyze, the vessel may experience shear loads at such locations, or even mixed-mode loadings, and these other modes could be more damaging. For these reasons, it was desired to examine the effects of both modes I and II loading on the PMMA and its weld joint.

Preferably, the stress intensity at the crack tip at the instance of failure should be a material parameter that is independent of specimen geometry. This dictates that the failure process zone must be small with respect to the sample such that the zone is not influenced by the boundaries of the specimen. The characteristic size of the process zone may be estimated by the plastic zone size, r_p , as determined by the following equation:

$$r_p = \frac{1}{\pi} \left(\frac{K_{Ic}}{\sigma_{ys}} \right)^2 \quad (1)$$

The value for the plastic zone size was computed for a critical stress intensity factor K_{Ic} found in the literature of $31.6 \text{ MPa}\cdot\text{mm}^{0.5}$ ($0.909 \text{ ksi}\cdot\text{in.}^{0.5}$) (ref. 7). A literature value for the yield stress for PMMA is about 44 MPa and this gives an estimate for the process zone size of 0.16 mm (0.006 in.). This length is

much less than the 6 mm (0.236 in.) specimen thickness, as well as all other specimen dimensions. Therefore, the process zone is sufficiently small, and plane strain conditions can be assumed when discussing the fracture toughness approach. The small process zone is also beneficial to the welded samples. Visual examination of the weld joint often showed bubbles in the joint. However, the bubbles were remote from the starter crack and sufficiently removed from the small process zone. Therefore, there is no interaction expected between the process zone and the bubbles. Thus, the bubbles are believed not to influence the results.

The analysis of the test results makes use of the Brazilian disk specimen calibration factors reported by Liu et al. (ref. 4) and adapted from Atkinson (ref. 5) for a crack length-to-disk diameter ratio of $(2a/2W) = 0.5$.

$$\begin{aligned} f_I\left(\frac{a}{W}, \varphi\right) &= \frac{K_I}{\frac{P}{2W} \cdot \sqrt{2a}} \\ f_{II}\left(\frac{a}{W}, \varphi\right) &= \frac{K_{II}}{\frac{P}{2W} \cdot \sqrt{2a}} \end{aligned} \quad (2)$$

In pure mode I the angle between the load axis and the notch is 0° and results in a value for $f_I(0.5, 0^\circ) = 1.069$. For mode II the angle is 22.5° resulting in a value for $f_{II}(0.5, 22.5^\circ) = 1.7$. Note that $f_{II}(0.5, 0^\circ) = f_I(0.5, 22.5^\circ) = 0$, and hence there is no contribution from shear in the 0° test or from normal loading in the 22.5° test. Uncracked ligament lengths on each end of the notch were generally measured on both sides of the specimen. They are reported in table III as L1, L2, L4, and L5, where L4 and L5 are measured on the back side of the disk and account for any skewness at the crack tip. The overall diameter of the each disk is reported as L3. Observe that the objective of achieving a/W ratios of exactly 0.5 was difficult to achieve as values ranged from 6 to 9 percent greater. This will have particular ramifications for the mode II configuration where zero mode I stress intensification is sensitive to crack length. Average starter crack length values were computed from these measurements and used to resolve K_{Ic} and K_{IIc} using equation (2). Table IV provides the maximum load and displacement at the point of load drop, which corresponds to crack initiation. These values are converted to load per unit thickness (P) in the appropriate formula. For reference, the load/notch angle is reported in tables IV and V to distinguish between modes I and II type fracture tests.

Table V reports the computed critical stress intensity values K_{Ic} and K_{IIc} ; the mean values and standard deviation are also included. The fracture toughness as given by the K_{Ic} values for both the welded and unwelded samples is similar. The mean values for K_{Ic} are about 20 percent greater ($37.1 \text{ MPa}\cdot\text{mm}^{0.5}$ ($1.07 \text{ ksi}\cdot\text{in.}^{0.5}$)) than the data reported in the literature, for example, $31.6 \text{ MPa}\cdot\text{mm}^{0.5}$ ($0.909 \text{ ksi}\cdot\text{in.}^{0.5}$) to $32.2 \text{ MPa}\cdot\text{mm}^{0.5}$ ($0.927 \text{ ksi}\cdot\text{in.}^{0.5}$) (refs. 7 and 8). This trend is in keeping with the tensile-strength test data of this investigation, which were also greater than those reported in the literature. An updated process zone size was also computed for these tests using the measured properties to doublecheck the validity of the plane strain assumption. The process zone size for a $37 \text{ MPa}\cdot\text{mm}^{0.5}$ ($1.065 \text{ ksi}\cdot\text{in.}^{0.5}$) material having a yield stress of about 52 MPa (7.54 ksi) is 0.16 mm (0.630 in.)—same as the initial estimate. Examination of the mode I fracture surface also indicates a brittle, glasslike fracture indicating that a plane strain assumption is valid. Standard deviation values for the unwelded specimens were only 2 to 4 percent of the mean values; this statistic increased to about 10 percent of the mean value for the welded specimens. This might be indicative of the variability of notch shape, weld line position or starter crack insertion. It should be reported that crack propagation in these specimens did not demonstrate an affinity for the weld line in contrast to the tensile tests. In other words, the weld was approximately as strong as the base material and other factors (such as stress state) determined the crack

direction. Indeed, the mode I fracture toughness for the welded material was only 1.3 percent greater than the unwelded material.

TABLE III.—PMMA BRAZILIAN DISKS GEOMETRY

Specimen no.	Welded/ unwelded	Angle, deg.	L1, mm	L2, mm	L3, mm	L4, mm	L5, mm
135	Unwelded	22.5	8.874	8.732	37.90	8.778	8.947
136	Unwelded	22.5	9.011	8.856	37.74	7.857	8.490
137	Unwelded	0	8.561	8.522	37.404	8.524	8.937
138	Unwelded	22.5	8.660	9.063	37.83	8.053	8.611
139	Unwelded	0	8.207	8.921	37.971		
140	Unwelded	0	8.849	8.583	37.963	8.773	8.313
141	Welded	22.5	8.450	8.924	37.936		
142	Welded	22.5	8.928	8.615	37.799		
143	Welded	0	9.35	9.481	37.91		
144	Welded	0	9.037	8.694	38.009		
152	Welded	0	8.291	8.160	37.95	8.212	8.238
153	Welded	0	8.752	9.206	37.938		
154	Welded	22.5	8.725	8.743	37.911		

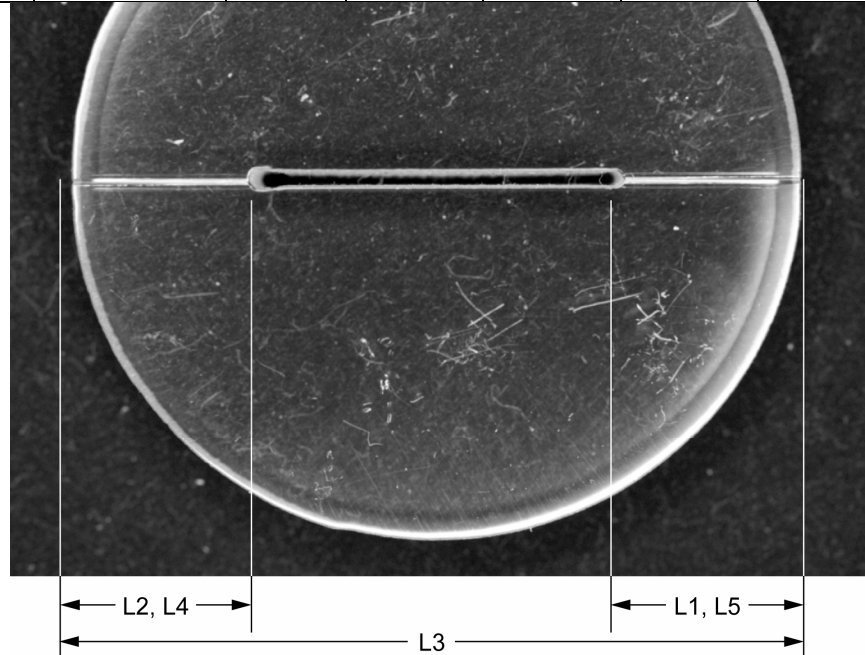


TABLE IV.—BRAZILIAN DISK TEST RESULTS

Specimen no.	Angle, deg.	Max. load, N	Max. displacement, mm
135	22.5	1463	0.404
136	22.5	1514	0.444
137	0	1654	0.471
138	22.5	1486	0.454
139	0	1753	0.559
140	0	1776	0.467
141	22.5	1579	0.533
142	22.5	1789	0.602
143	0	2081	0.523
144	0	1693	0.566
152	0	1594	0.457
153	0	1714	0.458
154	22.5	1895	0.576

TABLE V.—BRAZILIAN DISK FRACTURE TOUGHNESS

Specimen no.	Angle, deg.	K_{Ic} , MPa-mm ^{0.5}	K_{IIc} , MPa-mm ^{0.5}
Unwelded			
135	22.5	-----	49.5
136	22.5	-----	52.0
137	0	35.6	-----
138	22.5	-----	50.9
139	0	37.8	-----
140	0	38.0	-----
Mean	-----	37.1	50.8
STD	-----	1.35	1.23
Welded			
141	22.5	-----	53.8
142	22.5	-----	60.8
143	0	43.0	-----
144	0	36.0	-----
152	0	35.0	-----
153	0	36.2	-----
154	22.5	-----	64.5
Mean	-----	37.6	59.7
STD	-----	3.69	5.40

For the mode II tests, there is a larger disparity (approx. 17 percent) in the fracture toughness between the unwelded and welded materials—the welded material has higher fracture toughness. This could be explained if we examine the failure modes of the specimens. Unlike mode I cracks, which propagated parallel to the initial crack, the mode II tests initiated a kink crack at some angle ranging from 47° to 68° to the original notch plane. Figure 8 shows fractured samples for both types of cracks. Based on these observations the reported K_{IIc} fracture toughness values should not be considered as a true mode II fracture toughness for reasons that are explained below.

This phenomenon of crack kinking is well-known in the fracture mechanics literature and is ascribed to maximum energetic and maximum hoop stress effects on the direction of crack growth. In monolithic materials having isotropic failure criteria the crack will seek to propagate along a path that releases the maximum strain energy per unit crack growth. Analytically the strain energy release rate is $G(\alpha) \propto k_I^2(\alpha, a/W) + k_{II}^2(\alpha, a/W)$, where the small k indicates the stress intensity factors for an infinitesimal kinked crack at angle alpha. The differential

$$\frac{\partial G(\alpha)}{\partial \alpha} \tag{3}$$

may be used to determine the extrema of the energy release rate as a function of kink angle. It has been shown that the maximum energy release rate occurs at a kink angle of 70.5° for a pure mode II loaded crack. This kink angle corresponds to crack growth along a plane where the crack is extending in pure Mode I. For the crack to become trapped in the weld, the mode II fracture toughness of the weld would have to be significantly lower than the mode I fracture toughness, which is obviously not the case.

Still the measured kink angles do not agree with analysis. Also, if the kinked crack was failing at load levels consistent with the mode I fracture toughness the ratio K_{IIc}/K_{Ic} as calculated from table V should be about 0.86; looking at the mean values this ratio is 1.37 and 1.59 for the unwelded and weld materials, respectively. This aberration cannot be attributed to crack friction for closure of the Mode II crack behind the notch tip; the notch widths are too wide to close during loading. However, for a given included angle the mode I stress intensity factor is found to be a monotonically decreasing function of the (a/W) ratio (ref. 9). Our objective of achieving exactly 0.5 for the a/W ratio was difficult to achieve. Since the resulting crack geometries had a/W ratios that were greater than 0.5, the stress state ahead of the crack must be slightly compressive and will contribute to the distortional energy ahead of the shearing crack tip.

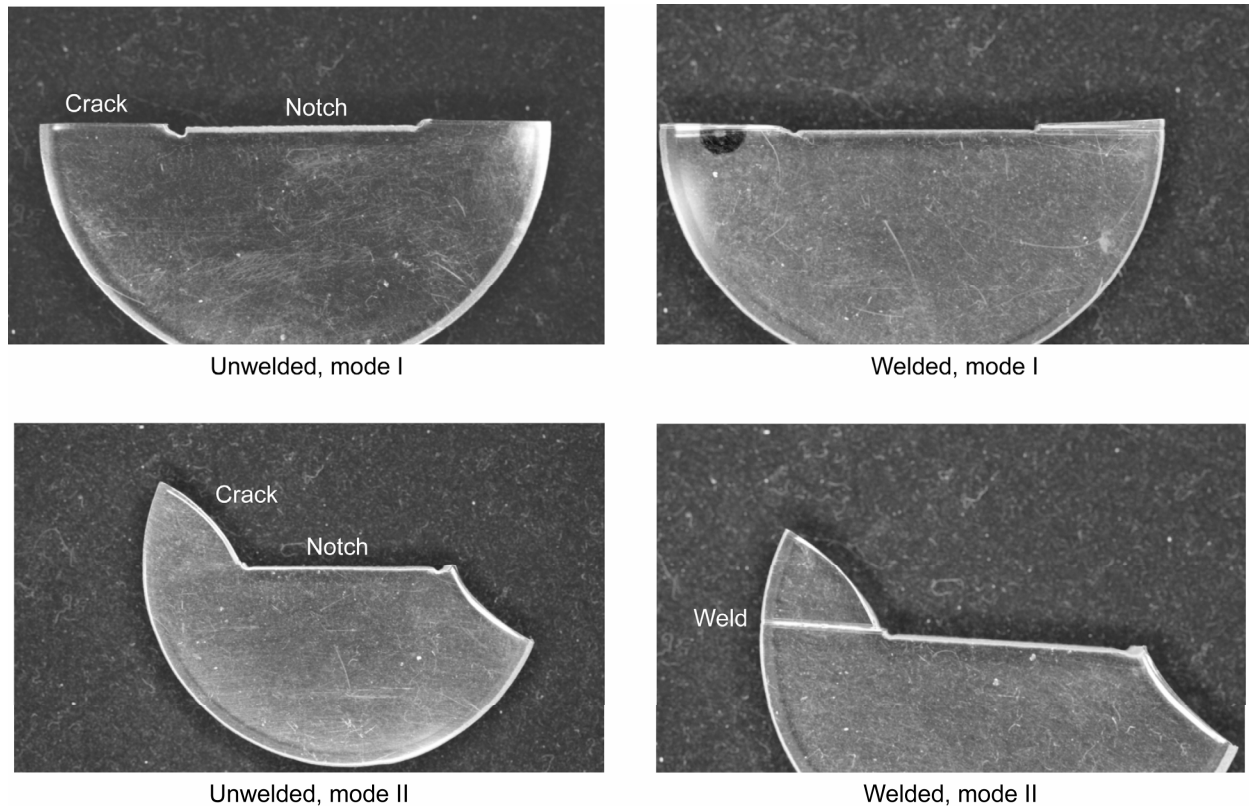


Figure 8.—Crack morphologies in the modes I and II Brazilian disks.

It is also known from analysis of modes I and II cracks in elastic-plastic materials that the plastic zone size in mode II “is up to five times larger than that in mode I” (ref. 10). Deviation from mode I to mode II-type growth is confronted with the need to do more plastic work to grow the crack. Note that Liu et al. (ref. 4) also report similar behavior for the mode II fracture response of monolithic epoxy disks. They suggest that it is the formation of shear bands at the tip of the crack, which explains the additional expenditure of energy in mode II tests. Certainly the combination of shear stress and compressive normal stresses would be expected to enhance the plastic work at the tip of the notch and delay the onset of the kinked crack. Inspection of the mode II unwelded specimens shows clearly the growth of a shear band ahead of the starter notch. The competing mechanism to release strain energy via the crack and the distorted process zone from the shear band are expected to influence the kink angle of the final failure. We did observe a shear band in tested specimens of unwelded, mode II samples, which ran from the starter notch crack tip and parallel to the center crack. However, efforts to image the shear band were fruitless.

Now if we return to the disparity between mode II fracture toughness values between the welded and unwelded samples, we can explain this through the above-mentioned mechanism. Assuming that the weld is slightly weaker than the surrounding material (this can indeed be observed by examining the tensile strengths of the welded vs. unwelded samples in fig. 6), the shear bands in the weld will absorb more energy than for the case of the shear bands in the unwelded material. Hence, a higher load will be needed to initiate the kinked mode I cracks for the welded samples.

Failure Prediction Using Fracture Mechanics

The data generated in this study show that the mode I fracture toughness is much less than that of the mode II. This suggests that a conservative lower bound for fracture toughness would be obtained by using the lowest limit for the mode I fracture toughness. All mixed mode loaded cracks are expected to have a

higher threshold for failure. Using $31.6 \text{ MPa}\cdot\text{mm}^{0.5}$ ($1.773 \text{ ksi}\cdot\text{in.}^{0.5}$) as the lowest mode I fracture toughness, the maximum ambient failure stress in the structure corresponds to 16 MPa (2.3 ksi) for a 1.0 mm (0.039 in.) edge crack. This stress will decrease as a function of the inverse square root of the initial flaw length, that is, the shorter the crack the higher the failure stress. This value may be used as a reference point when examining the critical mode I stress levels in the structure. Using realistic values for the dimensions and proof pressure, an analysis of the actual structure is given in the appendix. This analysis shows that there is a factor of three margin of safety for the worst-case conditions.

Conclusions

Using fundamental material and fracture mechanics, a pragmatic program of testing was designed to elicit the performance penalty in welded PMMA joints. The approach yielded valuable engineering design data in a timely and economical fashion. A number of interesting results were obtained that suggest routes for more rigorous fundamental studies in the future. Meanwhile, the primary engineering results are summarized below.

- (1) Tensile values for the unwelded samples agree with literature values for PMMA.
- (2) Soaking up to 8 weeks in either air or oil has no effect on tensile properties.
- (3) Weld defects (bubbles) have a significant and deleterious effect on both strength and strain to failure. The reduction in the properties scales with the size and distribution of the bubbles.
- (4) Notched samples significantly lowered strength and failure strain in a controlled fashion (predictable from fracture mechanics). However, the notched samples are not a worst-case scenario. Some bubble morphologies are more severe.
- (5) Any inherent weakness of the welded specimens was overshadowed by the deleterious effect of the notch on the strength of the specimen.
- (6) While for a noncracked sample the welded specimens were weaker, fracture tests did not show any inherent weakness of the welded specimens. The deleterious effect of the notch overwhelmed the lower strength of the weld.
- (7) The mode I fracture toughness K_{Ic} is 20 percent greater than values reported in the literature; values in the literature may be used as a lower bound for failure prediction in a first appraisal of the vessel.
- (8) Mode II fracture toughness is likely influenced by a slightly compressive stress ahead of the crack tip and the formation of shear bands from kinking mode I dominant cracks; mode II loading exhibits plastic zones parallel to the crack that are up to 5 times larger than in mode I cracks. As expected their values are much higher than would be predicted by energy theory and also higher than the mode I values.
- (9) A procedure for an upper-bound fracture mechanics analysis of the existing structure is presented. The analysis shows that the structure has a factor of three margin of safety.
- (10) Note that since this work was performed, the vessels have been launched upon various space shuttle missions and are now aboard the International Space Station. To date there have been no reports of leaking or cracked vessels and the experiments have run successfully.

Appendix

The structure in question is approximately a rectangular pressure vessel of PMMA that is solvent-bonded. The presence of notches at the bond joints suggests the need for an appraisal of the safety margin for crack-like flaws in these bonded joints. In a comparison of beam/plate theory, two- and three-dimensional finite element analyses, Thesken et al. (ref. 9) have shown that conservative upper bound estimates for the internal stresses in rectangular pressure vessels may be found by using a simply supported beam theory. According to the ASME Pressure Vessel Code Appendix 13 Vessels of Noncircular Cross Section, corner bending moments for rectangular vessels do not exceed the end moments for a rigidly fixed end beam. The span-to-depth ratio (L/h) in the structure controls the stress—internal pressure amplification factors. Choosing the largest (L/h) ratio for all pressure vessel walls sets an upper bound for the ambient wall stresses. The maximum normal stress on any flaw would be the superposition of the maximum bending stress and the maximum possible membrane stress as shown below. The maximum shear and membrane stress are equivalent in this upper bound estimate:

$$\begin{aligned}\sigma &= p \left[\frac{3}{4} \left(\frac{L}{h} \right)^2 + \frac{1}{2} \left(\frac{L}{h} \right) \right] \\ \tau &= p \frac{1}{2} \left(\frac{L}{h} \right)\end{aligned}\tag{4}$$

The values that correspond to the maximum stress location in this component are

$$\left(\frac{L}{h} \right) = \frac{35 \text{ mm}}{8 \text{ mm}}\tag{5}$$

which represent the largest span with the thinnest cross section at a glue reservoir. Equation (4) gives pressure multiplier factors for normal and shear stresses of 11.8 and 2.19, respectively. Assuming a 3-mm (0.118-in.) edge crack at the corner of the structure (this is based on a worst-case crack forming from the glue reservoir), these values should be inserted into the fracture mechanics equations to determine K_I and K_{II} , for example:

$$\begin{aligned}K_I &= 1.12 \sigma \sqrt{\pi a} \\ K_{II} &= 1.12 \tau \sqrt{\pi a}\end{aligned}\tag{6}$$

The predicted kink angle for the ratio of normal to shear stress on a 3-mm (0.118-in.) crack is 19.8°. The mode I stress intensity at this angle for a 0.241-MPa (35-psi) proof pressure is 10.3 MPa-mm^{0.5} (0.296 ksi-in.^{0.5}). The proof pressure of 0.241 MPa (35 psi) is 1.5 times the maximum design pressure as determined in ZIN Document CFE-DOC-025. This stress intensity is about 1/3 of the lowest value found in the literature. These simple fracture mechanics calculations suggest there is sufficient margin against failure for a 3.0-mm (0.118-in.) notch.

References

1. Standard Specification for Poly(Methyl Methacrylate) Acrylic Plastic Sheet. ASTM D 4802–02, ASTM International, West Conshohocken, PA, 2002.
2. Standard Test Method for Tensile Properties of Plastics. ASTM D 638–03, ASTM International, West Conshohocken, PA, 2003.
3. Omnexus Polymer Center. <http://www.omnexus.com/tc/polymerscenter/index.aspx> Accessed June 14, 2007.
4. Liu, C.; Huang, Y.; and Stout, M.G.: Enhanced Mode-II Fracture Toughness of an Epoxy Resin Due to Shear Banding. *Acta Mater.*, vol. 46, no. 16, 1998, pp. 5647–5661.
5. Atkinson, C.; Smelser, R.E.; and Sanchez, J.: Combined Mode Fracture Via the Cracked Brazilian Disk Test. *Int. J. Fract.*, vol. 18, no. 4, 1982, pp. 279–291.
6. Gomez, F.J.; and Elices, M.: Fracture of Components With V-Shaped Notches. *Eng. Fract. Mech.*, vol. 70, no. 14, 2003, pp. 1913–1927.
7. Dunn, M.L.; Suwito, W.; and Cunningham, S.: Fracture Initiation at Sharp Notches: Correlation Using Critical Stress Intensities. *Int. J. Solids Struct.*, vol. 34, no. 29, 1997, pp. 3873–3883.
8. Suresh, S.: *Fatigue of Materials*. Cambridge University Press, Cambridge, New York, NY, 1991.
9. Thesken, J.C., et al.: Design Analysis of a Composite Combustion Chamber Support. Presented at the 49th International SAMPE Symposium and Exhibition, Long Beach, CA, 2004.
10. Weislogel, M.: The Capillary Flow Experiments: Handheld Fluids Experiments for International Space Station. AIAA–2004–1148, 2004.

REPORT DOCUMENTATION PAGE

Form Approved
OMB No. 0704-0188

The public reporting burden for this collection of information is estimated to average 1 hour per response, including the time for reviewing instructions, searching existing data sources, gathering and maintaining the data needed, and completing and reviewing the collection of information. Send comments regarding this burden estimate or any other aspect of this collection of information, including suggestions for reducing this burden, to Department of Defense, Washington Headquarters Services, Directorate for Information Operations and Reports (0704-0188), 1215 Jefferson Davis Highway, Suite 1204, Arlington, VA 22202-4302. Respondents should be aware that notwithstanding any other provision of law, no person shall be subject to any penalty for failing to comply with a collection of information if it does not display a currently valid OMB control number.

PLEASE DO NOT RETURN YOUR FORM TO THE ABOVE ADDRESS.

1. REPORT DATE (DD-MM-YYYY) 01-08-2007		2. REPORT TYPE Technical Memorandum		3. DATES COVERED (From - To)	
4. TITLE AND SUBTITLE Polymethylmethacrylate (PMMA) Material Test Results for the Capillary Flow Experiments (CFE)				5a. CONTRACT NUMBER	
				5b. GRANT NUMBER	
				5c. PROGRAM ELEMENT NUMBER	
6. AUTHOR(S) Lerch, Bradley, A.; Thesken, John, C.; Bunnell, Charles, T.				5d. PROJECT NUMBER	
				5e. TASK NUMBER	
				5f. WORK UNIT NUMBER WBS-22-376-10-30-04	
7. PERFORMING ORGANIZATION NAME(S) AND ADDRESS(ES) National Aeronautics and Space Administration John H. Glenn Research Center at Lewis Field Cleveland, Ohio 44135-3191				8. PERFORMING ORGANIZATION REPORT NUMBER E-16049	
9. SPONSORING/MONITORING AGENCY NAME(S) AND ADDRESS(ES) National Aeronautics and Space Administration Washington, DC 20546-0001				10. SPONSORING/MONITORS ACRONYM(S) NASA	
				11. SPONSORING/MONITORING REPORT NUMBER NASA/TM-2007-214835	
12. DISTRIBUTION/AVAILABILITY STATEMENT Unclassified-Unlimited Subject Category: 27 Available electronically at http://gltrs.grc.nasa.gov This publication is available from the NASA Center for AeroSpace Information, 301-621-0390					
13. SUPPLEMENTARY NOTES					
14. ABSTRACT In support of the Capillary Flow Experiments (CFE) program, several polymethylmethacrylate (PMMA) flight vessels were constructed. Some vessels used a multipiece design, which was chemically welded together. Due to questions regarding the effects of the experiment fluid (silicone oil) on the weld integrity, a series of tests were conducted to provide evidence of the adequacy of the current vessel design. Tensile tests were conducted on PMMA samples that were both in the as-received condition, and also aged in air or oil for up to 8 weeks. Both welded and unwelded samples were examined. Fracture of the joints was studied using notched tensile specimens and Brazilian disk tests. Results showed that aging had no effect on tensile properties. While the welded samples were weaker than the base parent material, the weld strength was found to be further degraded by bubbles in the weld zone. Finally a fracture analysis using the worst-case fracture conditions of the vessel was performed, and the vessel design was found to have a factor of three safety margin.					
15. SUBJECT TERMS Polymethylmethacrylate; Strength; Notches; Glue joints; Brazilian disk test					
16. SECURITY CLASSIFICATION OF:			17. LIMITATION OF ABSTRACT	18. NUMBER OF PAGES 22	19a. NAME OF RESPONSIBLE PERSON STI Help Desk (email:help@sti.nasa.gov)
a. REPORT U	b. ABSTRACT U	c. THIS PAGE U			19b. TELEPHONE NUMBER (include area code) 301-621-0390

